screw component. By using the method for determining the Burgers vector proposed by Tanaka, Terauchi & Kaneyama (1988), the Burgers vector is determined to be $\frac{1}{2}[011]$ or $\frac{1}{2}[01\bar{1}]$.

References

CARPENTER, R. W. & SPENCE, J. C. H. (1982). *Acta Cryst.* A**38**, 55-61.

CHERNS, D., KIELY, C. J. & PRESTON, A. R. (1988). *Ultramicroscopy*, **24**, 355-369.

CHERNS, D. & PRESTON, A. R. (1986). Proc. XIth Int. Congr. on Electron Microscopy, Kyoto, Japan, pp. 721-722.

HIRSCH, P., HOWIE, A., NICHOLSON, R. B., PASHLEY, D. W. & WHELAN, M. J. (1977). *Electron Microscopy of Thin Crystals*, pp. 164, 178, 198, 250. Huntington, New York: Robert E. Krieger.

JIAO, S., ZOU, H. & WANG, R. (1987). *J. Chin. Electron Microsc. Soc.* **6**, 42-47. (In Chinese.)

LU, G., WEN, J. G., ZHANG, W. & WANG, R. (1990). *Acta Cryst.* A**46**, 103-112.

TANAKA, M., TERAUCHI, M. & KANEYAMA, T. (1988). *Convergent-Beam Electron Diffraction* II, pp. 160-185. Tokyo: JEOL-Maruzen.

WEN, J., WANG, R. & LU, G. (1989). *Acta Cryst.* A**45**, 422-427.

Acta Cryst. (1991). A**47**, 39-44

Effects of Crystal-Surface Inclination on X-ray Multiple Diffraction: Intensity Variation and Phase Determination

BY KUANG-CHIH LEE AND SHIH-LIN CHANG

Department of Physics, National Tsing Hua University, Hsinchu, Taiwan 30043

(*Received* 21 *July* 1989; *accepted* 3 *September* 1990)

Abstract

Effects of crystal-surface inclination on the intensities of X-ray *Umweganregung* multiple diffractions are investigated for perfect silicon crystals. The intensity variations of the multiply diffracted beams due to the surface inclination are accounted for in terms of three-beam dynamical calculations. Quantitative phase determination direct from the intensity profile analysis is also carried out. It is found that the phase determination is not affected by the crystal-surface inclination. This conclusion is also supported by the analysis of the profile asymmetry.

1. Introduction

X-ray multiple diffraction takes place when several sets of atomic planes are simultaneously brought into position to diffract an incident X-ray beam. The coherent dynamical interaction among the multiply diffracted waves, which governs the diffraction intensities, has long been investigated for Borrmann (transmission) geometry (Borrmann & Hartwig, 1965; Saccocio & Zajac, 1965; Hildebrandt, 1967; Joko & Fukuhara, 1967; Ewald & Heno, 1968; Uebach & Hildebrandt, 1969; Balter, Feldman & Post, 1971; Umeno & Hildebrandt, 1975; Post, Chang & Huang, 1977; Høier & Aanestad, 1981; Campos & Chang, 1986; and many others), and for Renninger (reflection) geometry (Renninger, 1937; Colella, 1974; Chapman, Yoder & Colella, 1981; Chang, 1981, 1982; Juretschke, 1982*a*, *b*; Hümmer & Billy, 1982, 1986; Post, 1983; Post, Nicolosi & Ladell, 1984; Shen, 1986; Thorkildsen, 1987; Chang & Tang, 1988; and many others). Besides, the extraction of phase information from the intensity distribution of multiple diffractions has recently become one of the major themes in this particular area of research. Reports on this subject include articles by Hart & Lang (1961), Ewald & Heno (1968), Colella (1974), Post (1977), Jagodzinski (1980), Chapman, Yoder & Colella (1981), Chang (1981, 1982), Høier & Aanestad (1981), Juretschke (1982*a*), Hümmer & Billy (1982), Post (1983), Post, Nicolosi & Ladell (1984), Shen (1986) and Mo, Haubach & Thorkildsen (1988) for centrosymmetric crystals, and by Juretschke (1982*b*), Chang & Valladares (1985), Hümmer & Billy (1986), Shen & Colella (1988), Tang & Chang (1988) and Hümmer, Weckert & Bondza (1989) for noncentrosymmetric crystals.

Very recently, a quantitative phase-determination procedure using three-beam diffraction-intensity profiles has been proposed (Chang & Tang, 1988). Experimental phase determination has also been realized for perfect-crystal plates (Tang & Chang, 1988). In that approach, the intensity due to dynamical interaction, which may be separated from the total intensity distribution, is directly related to the phases of the involved structure-factor multiplets. As far as the dynamical effect in multibeam diffraction is concerned, the excitation of the dispersion surface governed by the crystal boundary plays a key role in the allocation of the total energy into the diffracted waves. Namely, the diffraction intensities depend also on the crystal boundary. Recently, Kov'ev & Deigen (1987) have reported the intensity variation over

0108-7673/91/010039-06$03.00

angular deviations in the Bragg angle of a relatively strong *Aufhellung* (Renninger, 1937) three-beam diffraction in an asymmetrically cut crystal. It is, however, the purpose of this article to investigate systematically the effects of inclined crystal surfaces on the intensities of *Umweganregung* (Renninger, 1937) multiple diffractions in a 360° azimuthal rotation around a given reciprocal-lattice vector. The connection between the crystal boundary and the accuracy of the quantitative phase determination is also investigated and discussed.

We concentrate on the cases involving three-beam *Umweganregung* (Renninger, 1937) diffractions from the (centrosymmetric) crystals of silicon. The clear asymmetric intensity profiles, due to the triplet phases of 0 and 180°, facilitate the investigation.

2. Experimental

The experimental arrangement reported by Tang & Chang (1988) was adopted. A Cu target and a filament of 3000×300 μm were used. The focal size of the incident beam was about 300×300 μm. The angular beam divergence was 0·033° in both vertical and horizontal directions. The beam size at the crystal was about 1·73 mm in diameter.

Several [111]-cut plate-like perfect silicon crystals with the surface inclination angles of 0, 10 and 20° with respect to the (111) planes were prepared. The crystal surfaces were polished with 0·3 μm Al_2O_3 powder and then etched with CP-4A solution [$HF(1):HNO_3(4):CH_3COOH(2)$]. The direction of inclination is along $[1\bar{1}0]$. The areas of the crystal surfaces irradiated by the incident X-rays were always smaller than the total crystal surfaces.

The experiment is performed by setting the crystal for 222 reflection, the primary reflection G, and then rotating the crystal around the reciprocal-lattice vector $\mathbf{g}$ of the 222 reflection to bring additional sets of atomic planes (of the secondary reflection L) in a position to satisfy Bragg's law. Thus, multiple diffraction takes place. The interaction among the diffracted waves gives rise to the intensity variation on the background of the 222 reflection. A scintillation counter is used to monitor this intensity variation for the 222 reflection.

The geometric relation among the crystal surface normal, indicated as the downward unit vector $\hat{\mathbf{n}}_e$, and the directions of the diffracted beams, represented by the wavevectors $\mathbf{k}_0$, $\mathbf{k}_G$ and $\mathbf{k}_L$ in vacuum, is depicted in Fig. 1. La is the Laue point, the center of the Ewald sphere, such that $k_0 = k_G = k_L = k = 1/\lambda$. λ is the wavelength of the X-rays used. **OG** (=**g**) and OL (=**l**) are the reciprocal-lattice vectors of the G and L reflections. Here, instead of rotating the crystal, we rotate the X-ray beam around the crystal. Hence, the La point is rotated around **g**, while the crystal is fixed. The x, y and z axes are chosen to be along the $[1\bar{1}0]$, $[11\bar{2}]$ and [111] directions. θ_0 and θ_L are the polar angles and φ_0 and φ_L are the azimuthal angles of $-\mathbf{k}_0$ and **l**, respectively. $\hat{\mathbf{n}}_e$ is in the XZ plane. The angle φ_n between **g** and $\hat{\mathbf{n}}_e$ is $180°-\alpha$. Because of the relative rotation of the point La with respect to the crystal, $\varphi_0 = -\varphi$.

In terms of a spherical coordinate system, the vectors $\hat{\mathbf{n}}_e$, **g**, **l**, $\mathbf{k}_0$, $\mathbf{k}_G$ and $\mathbf{k}_L$ are expressed as

$$\hat{\mathbf{n}}_e = (-\sin\alpha, 0, -\cos\alpha) \tag{1}$$

$$\mathbf{g} = g(0, 0, 1) \tag{2}$$

$$\mathbf{l} = l(\sin\theta_L\cos\varphi_L, \sin\theta_L\sin\varphi_L, \cos\theta_L) \tag{3}$$

$$\mathbf{k}_0 = k(-\sin\theta_0\cos\varphi_0, -\sin\theta_0\sin\varphi_0, -\cos\theta_0) \tag{4}$$

$$\mathbf{k}_G = k(-\sin\theta_G\cos\varphi_0, -\sin\theta_0\sin\varphi_0, \cos\theta_0) \tag{5}$$

$$\begin{aligned}\mathbf{k}_L = (&l\sin\theta_L\cos\varphi_L - k\sin\theta_0\sin\varphi_0,\\ &l\sin\theta_L\sin\varphi_L - k\sin\theta_0\sin\varphi_0,\\ &l\cos\theta_L - k\cos\theta_0).\end{aligned} \tag{6}$$

At the exact three-beam diffraction peak position, $\varphi_0 = \varphi_p$ and $k_L = k$. From (6) and the relation $\theta_0 = 90° - \theta_B$ (θ_B is the Bragg angle of the G reflection), we obtain (Cole, Chambers & Dunn, 1962)

$$\varphi_p = \varphi_L \pm \beta \tag{7}$$

where

$$\beta = \arccos\left[\frac{l/2k - \cos\theta_L\sin\theta_B}{\sin\theta_L\cos\theta_B}\right]. \tag{8}$$

The two φ_p's given in (7) are the two positions, the IN and OUT positions, at which the Ewald sphere touches the point L. The IN position corresponds to the situation where the relative motion brings the point L towards the Ewald sphere, and the OUT position to that for the point L leaving the Ewald sphere.

To reveal the crystal-boundary effect on the intensities of multiple diffractions, slow step scans

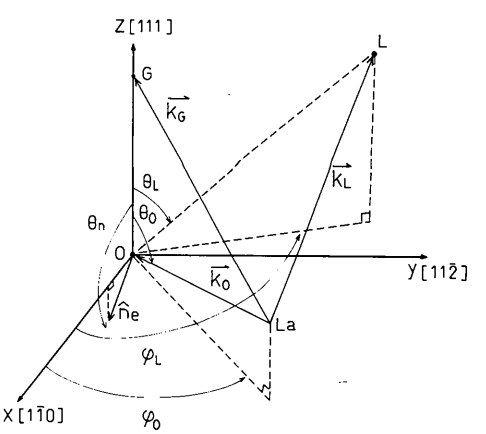

Fig. 1. Geometry of a three-beam (0, G, L) diffraction in reciprocal space.

(φ scans around [222]) are carried out for the following well resolved strong three-beam diffractions: $\{113/11\bar{1}\}$, $\{11\bar{1}/113\}$, $\{133/1\bar{1}\bar{1}\}$, $\{1\bar{1}\bar{1}/133\}$ and $\{\bar{1}33/3\bar{1}\bar{1}\}$ for Cu $K\alpha_1$ and Cu $K\beta$. The indices before and after the slashes indicate the secondary reflection L and the coupling $G-L$ reflection, respectively. The bracket $\{\}$ stands for the family of all the permuted hkl reflections. The step width of the scans is 0·01°. The counting time is so chosen that the error in the counting statistics is less than 1%. The relative intensity ratios, $I'_G=(I_3-I_2)/I_2$, are plotted against the azimuthal φ angles, where I_2 is the two-beam intensity of 222 and I_3 the three-beam intensity. Figs. 2(a)-(d) are such plots for Si $\{113/11\bar{1}\}$ with $\alpha=0$, 10 and 20° for Cu $K\alpha_1$ radiation. $\varphi=0$ corresponds to the angular position at which the $[1\bar{1}0]$ direction is coincident with the plane of incidence of the 222 reflection. The diffractions at the IN positions are marked by stars. In Fig. 2(a), some of the diffraction profiles are shown for illustration. The well defined intensity asymmetries near the profile tails are clearly observed. Fig. 2(b) shows the peak intensities of all the $\{113/11\bar{1}\}$ three-beam diffractions. The tails of the profiles are not shown to save space. The peak intensities of these three-beam cases are almost the same for $\alpha=0°$. Only the 113 and $1\bar{1}1$ cases have slightly higher peak intensities than the others. This is probably due to the inhomogeneity of the incident beam.

Figs. 2(c) and (d) are the three-beam diffraction profiles displayed over the 360° azimuth for $\alpha=10$ and 20°, respectively. The decrease of peak intensity asymmetry near the profile tails is still clearly seen. Similar behavior for the diffraction profiles of $\{113/11\bar{1}\}$ for Cu $K\beta$ (which are not shown here) is also observed.

The intensity profiles of the three-beam diffraction $\{133/1\bar{1}\bar{1}\}$ for Cu $K\beta$ are shown in Figs. 3(a) and (b) for $\alpha=10$ and 20°. Those profiles for $\alpha=0°$, having uniform peak intensities, are not shown. The intensity asymmetry, although not as pronounced as in Fig. 2, remains observable. The intensity decrease takes place every 60° in azimuth. As α increases, the effect becomes more pronounced. All these features are qualitatively reproduced by calculations given in Fig. 4.

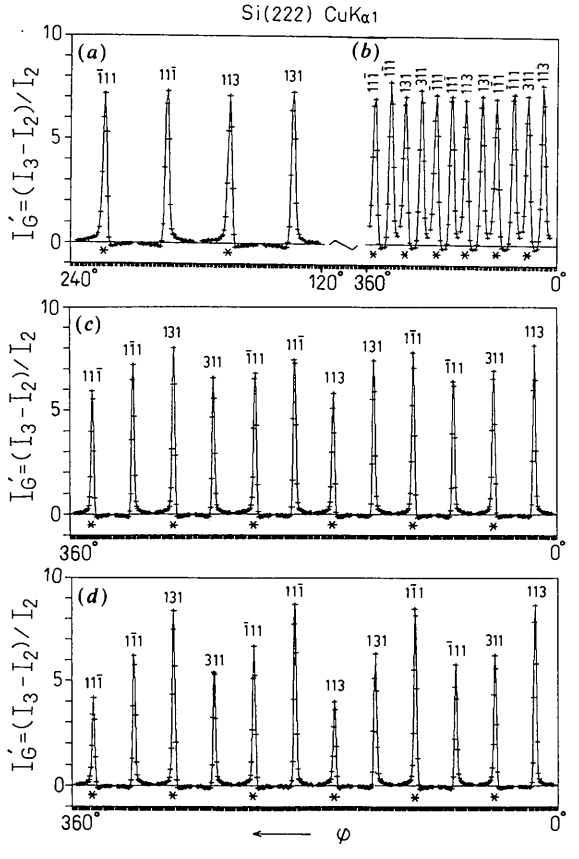

Fig. 2. Slow scans of $\{113/11\bar{1}\}$ and $\{11\bar{1}/113\}$ three-beam diffractions for Cu $K\alpha_1$ (the full widths at half maxima are about 0·05°): (a) intensity profiles for $\alpha=0°$; (b) peak intensities for $\alpha=0°$; (c) intensity profiles for $\alpha=10°$; (d) intensity profiles for $\alpha=20°$.

3. Data analysis and phase determination

As stated in the *Introduction*, the three-beam diffraction intensity is dependent on the crystal boundary and the involved triplet invariant phase. In the following, we first calculate the diffraction intensities for the varying crystal boundary as φ changes, assuming that the triplet phase δ_3 is the phase calculated from the known crystal structure. We then carry out a quantitative determination of phases using the

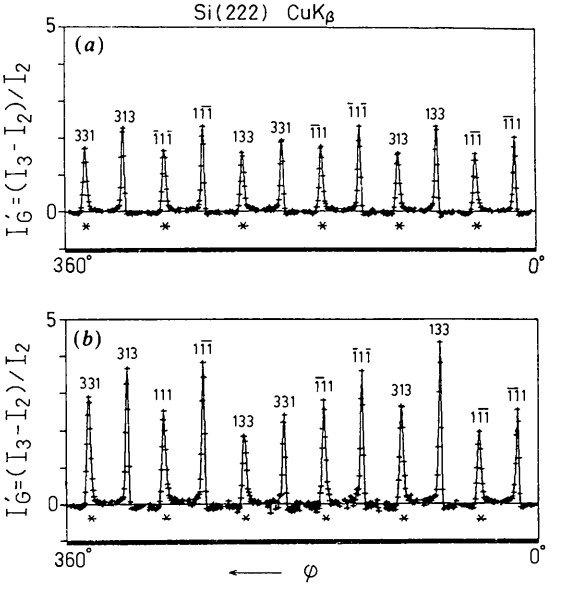

Fig. 3. Slow scans of $\{133/1\bar{1}\bar{1}\}$ and $\{1\bar{1}\bar{1}/133\}$ three-beam diffraction for Cu $K\beta$: (a) $\alpha=10°$ and (b) $\alpha=20°$.

intensity profiles and examine how the crystal boundary affects the determined phase values.

(*a*) *Intensity calculations*

To explain the intensity variation observed, due to the crystal boundary effect, the dynamical theory of X-ray diffraction for three-beam cases is employed.

The fundamental equation of wavefield for a three-beam (0, *G*, *L*) diffraction can be written as (see, for example, Chang, 1984)

$$\begin{pmatrix} 2\xi_0 & 0 & p_\sigma\chi_{\bar{G}} & 0 & d_2\chi_{\bar{L}} & 0 \\ 0 & 2\xi_0 & 0 & p_\pi\chi_{\bar{G}} & d_1\chi_{\bar{L}} & d_3\chi_{\bar{L}} \\ p_\sigma\chi_G & 0 & 2\xi_G & 0 & d_2\chi_{G-L} & 0 \\ 0 & p_\pi\chi_G & 0 & 2\xi_G & d'_1\chi_{G-L} & d'_3\chi_{G-L} \\ d_2\chi_L & d_1\chi_L & d_2\chi_{L-G} & d'_1\chi_{L-G} & 2\xi_L & 0 \\ 0 & d_3\chi_L & 0 & d'_3\chi_{L-G} & 0 & 2\xi_L \end{pmatrix} \begin{pmatrix} E_{\sigma 0} \\ E_{\pi 0} \\ E_{\sigma G} \\ E_{\pi G} \\ E_{\sigma L} \\ E_{\pi L} \end{pmatrix} = [0], \tag{9}$$

where the resonance failures $2\xi_H$'s are defimed as

$$2\xi_H = \chi_0 - (K_H^2 - k^2)/k^2 \tag{10}$$

for $H=0$, G and L. $E_{\sigma H}$ and $E_{\pi H}$ are the σ and π components of the wavefield amplitudes of the H reflection. p's and d's are the polarization factors defined as follows:

$$\begin{aligned} p_\sigma &= \hat{\boldsymbol{\sigma}}_0 . \hat{\boldsymbol{\sigma}}_0 = 1 \\ p_\pi &= \hat{\boldsymbol{\pi}}_0 . \hat{\boldsymbol{\pi}}_0 = \cos 2\theta_B \\ d_1 &= \hat{\boldsymbol{\pi}}_0 . \hat{\boldsymbol{\sigma}}_L = -\sin\psi \sin(\theta_B - t) \\ d_2 &= \hat{\boldsymbol{\sigma}}_0 . \hat{\boldsymbol{\sigma}}_L = \hat{\boldsymbol{\sigma}}_G . \hat{\boldsymbol{\sigma}}_L = \cos\psi \\ d_3 &= \hat{\boldsymbol{\pi}}_0 . \hat{\boldsymbol{\pi}}_L = \cos(\theta_B - t) \\ d'_1 &= \hat{\boldsymbol{\pi}}_G . \hat{\boldsymbol{\sigma}}_L = \sin\psi \sin(\theta_B + t) \\ d'_3 &= \hat{\boldsymbol{\pi}}_G . \hat{\boldsymbol{\pi}}_L = \cos(\theta_B + t) \\ \hat{\boldsymbol{\sigma}}_0 . \hat{\boldsymbol{\pi}}_0 &= \hat{\boldsymbol{\sigma}}_0 . \hat{\boldsymbol{\pi}}_L = \hat{\boldsymbol{\pi}}_0 . \hat{\boldsymbol{\sigma}}_G = \hat{\boldsymbol{\sigma}}_G . \hat{\boldsymbol{\pi}}_L = 0, \end{aligned} \tag{11}$$

where $\hat{\boldsymbol{\sigma}}$'s and $\hat{\boldsymbol{\pi}}$'s are the unit vectors of the corresponding σ and π polarization. Referring to Fig. 1, $\hat{\boldsymbol{\sigma}}_0$ and $\hat{\boldsymbol{\sigma}}_G$ are perpendicular to the $0G$La plane and $\hat{\boldsymbol{\pi}}_0$ and $\hat{\boldsymbol{\pi}}_G$ lie in the plane $0G$La. $\hat{\boldsymbol{\pi}}_L$ is chosen to be normal to $\hat{\boldsymbol{\sigma}}_0$ and $\hat{\boldsymbol{\sigma}}_G$ and parallel to the $0G$La plane. All the $\hat{\boldsymbol{\sigma}}$'s are perpendicular to the corresponding $\mathbf{K}$'s. t is the angle between the wavevector $\mathbf{K}_0$ and the projected $\mathbf{K}_L$ onto the $0G$La plane. ψ is defined, according to Fig. 1, as

$$\psi = \varphi_L - \varphi_0.$$

χ_0 is equal to ΓF_0, where $\Gamma = -r_e\lambda^2/\pi V$ and F_0 is the modulus of the structure factor of the 0 reflection. r_e is the classical radius of the electron and V the volume of the crystal unit cell. Equation (9) involves the invariant phase δ_3 of the structure-factor triplet $F_{\bar{G}}F_LF_{G-L}$.

By considering small angular deviations, $\Delta\varphi$ in azimuth and $\Delta\theta$ in θ_B, and the accommodation $k\zeta$ along $\hat{\mathbf{n}}_e$, the wavevector $\mathbf{K}_H$ inside the crystal can be expressed as

$$\begin{aligned} \mathbf{K}_H = k\hat{\mathbf{k}}_H - k\zeta\hat{\mathbf{n}}_e + (\Delta\theta)[(\hat{\mathbf{k}}_G \times \hat{\mathbf{k}}_0) \times \hat{\mathbf{k}}_0] \\ + (\Delta\varphi)\hat{\mathbf{z}} \times \hat{\mathbf{k}}_0 \end{aligned} \tag{12}$$

for $H=0$, G and L. Neglecting the second-order terms in ζ, $\Delta\theta$ and $\Delta\varphi$, the corresponding $2\xi_H$'s are

$$2\xi_H \simeq \chi_0 + 2\zeta\gamma_H + (\Delta\theta)a_H + (\Delta\varphi)b_H, \tag{13}$$

where

$$a_H = -2\hat{\mathbf{k}}_H . [(\hat{\mathbf{k}}_G \times \hat{\mathbf{k}}_0) \times \hat{\mathbf{k}}_0] \tag{14}$$

$$b_H = -2\hat{\mathbf{K}}_H . [\hat{\mathbf{z}} \times \hat{\mathbf{k}}_0], \tag{15}$$

γ_H is the direction cosine of $\mathbf{K}_H$ with respect to $\hat{\mathbf{n}}_e$.

As usual, (9) can be solved as an eigenvalue problem. The secular equation describes the dispersion surface. The eigenvectors give the ratios among the E's. The absolute values of the wavefield amplitudes

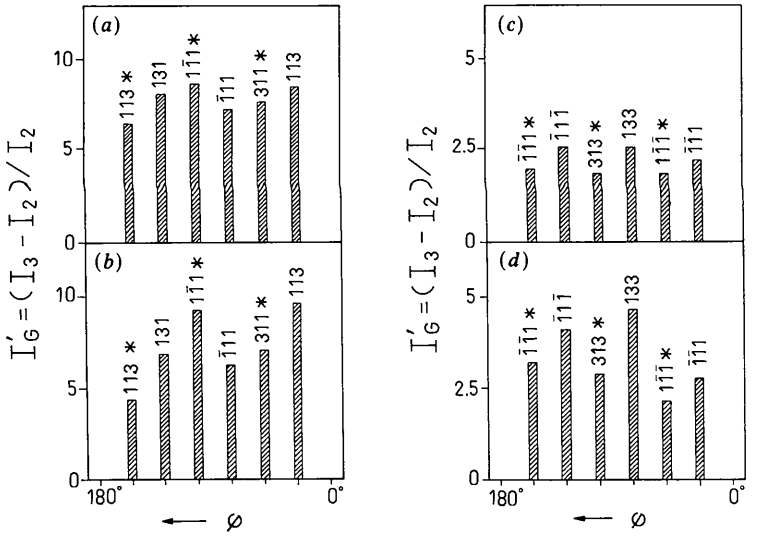

Fig. 4. Calculated relative intensity ratios, $I'_G = (I_3 - I_2)/I_2$ for $\{113/11\bar{1}\}$ and $\{11\bar{1}/113\}$ three-beam diffractions for Cu $K\alpha_1$ with (*a*) $\alpha = 10°$ and (*b*) $\alpha = 20°$; and the I'_G for $\{133/1\bar{1}\bar{1}\}$ and $\{1\bar{1}\bar{1}/133\}$ three-beam diffractions for Cu $K\beta$ with (*c*) $\alpha = 10°$ and (*d*) $\alpha = 20°$.

can be determined from the boundary conditions. Intensities can then be calculated accordingly. This calculation procedure is straightforward and will not be repeated here (see Chang, 1984; Colella, 1974).

Fig. 4 shows the calculated integrated intensity ratios (over $\Delta\theta$ and $\Delta\varphi$) of the three-beam $\{113/11\bar{1}\}$ and $\{11\bar{1}/113\}$ for Cu $K\alpha_1$ and Cu $K\beta$ for $0<\varphi<180°$. The angular ranges in $\Delta\theta$ and $\Delta\varphi$ for integration are 120 arc s. Agreement between the calculated (Fig. 4) and the experimental I'_G (Figs. 2 and 3) is obtained.

(*b*) *Quantitative phase determination*

According to Chang & Tang (1988), the relative intensity distribution $I'_G(\Delta\varphi)$ of a three-beam (0, *G*, *L*) diffraction can be written as

$$I'_G(\Delta\varphi)=[I_3(\Delta\varphi)-I_2(\Delta\varphi)]/[I_2(\Delta\varphi)]$$
$$=I_D(\Delta\varphi)+I_K(\Delta\varphi), \quad (16)$$

where $I'_G(\Delta\varphi)$, a function of $\Delta\varphi$, is a convolution of the intrinsic diffraction profile, the crystal mosaic distribution and the instrumental broadening function. The dynamical intensity I_D and the kinematical intensity I_K are

$$I_D=2Pa_1Q[2(\Delta\varphi)\cos\delta_3-\eta_T\sin\delta_3] \quad (17)$$

$$I_K=a_2P^2\eta_T/\eta_i, \quad (18)$$

where

$$P=|\Gamma|kL_FQ(|F_{G-L}||F_L|/|F_G|) \quad (19)$$

$$Q=1/[(\Delta\varphi)^2+(\eta_T/2)^2]^{1/2} \quad (20)$$

$$L_F=k/W \quad (21)$$

$$W=kl\sin\theta_L\sin\beta\cos\theta_B. \quad (22)$$

L is the Lorentz factor for three-beam diffraction. η_i and η_T are the intrinsic diffraction peak width and the total experimental peak width at half maximum, respectively:

$$\eta_i=k^2|\chi''_0|/W \quad (23)$$

$$\eta_T=\eta_i+\eta_B+\eta_M, \quad (24)$$

where η_B and η_M are the average beam broadening and the mosaic spread. a_1 and a_2 are the polarization factors defined in the article of Chang & Tang (1988). The parameter P which is different from that given previously is redefined in (19) for convenience.

The relative intensity distributions $I'_G(\Delta\varphi)$ are the experimentally obtained diffraction profiles shown in Figs. 2 and 3. For centrosymmetric crystals, $\delta_3\simeq 0$ or 180°. Referring to (17), $I_D=0$ at the exact three-beam diffraction position $\Delta\varphi=0$, namely $\varphi=-\varphi_p$ (provided that the error in $\Delta\varphi$ is so small that it can be neglected). The corresponding kinematical intensity is equal to the measured peak intensity $I'_G(\Delta\varphi)=0$. According to (18), I_K is a Lorentzian. With the $I_K(\Delta\varphi=0)=I'_G(\Delta\varphi=0)$ as the peak value and the experimental peak width η_T as the full width at half maximum, a Lorentzian can be constructed for the $I_K(\Delta\varphi)$. Consequently, the dynamical intensity distribution $I_D(\Delta\varphi)$ is readily defined as

$$I_D(\Delta\varphi)=I'_G(\Delta\varphi)-I'_G(\Delta\varphi=0)$$
$$\times\{(\eta_T/2)/[(\Delta\varphi)^2+(\eta_T/2)^2]^{1/2}\}. \quad (25)$$

Alternatively, taking the experimental facts into account, I_K may be a Gaussian. The $I_D(\Delta\varphi)$ then takes the form

$$I_D(\Delta\varphi)=I'_G(\Delta\varphi)-I'_G(\Delta\varphi=0)$$
$$\times\exp\{-[\Delta\varphi/1{\cdot}201(\eta_T/2)]^2\}. \quad (26)$$

The triplet phase δ_3 can then be determined according to Chang & Tang (1988) *via*

$$\cos\delta_3-\sin\delta_3=I_+/(2Pa_1QW)|_{\Delta\varphi=\eta_T/2} \quad (27a)$$

$$-\cos\delta_3-\sin\delta_3=I_-/(2Pa_1QW)|_{\Delta\varphi=-\eta_T/2}, \quad (27b)$$

where

$$I_\pm=I_D(\Delta\varphi=\pm\eta_T/2). \quad (28)$$

Calculation of δ_3 is carried out for each three-beam diffraction profile. There are 24 profiles for each three-beam family. The maximum and minimum calculated values of δ_3 for each three-beam family are listed in Table 1 for $\{113/11\bar{1}\}$ Cu $K\alpha_1$, $\{113/11\bar{1}\}$ Cu $K\beta$, $\{133/1\bar{1}\bar{1}\}$ Cu $K\beta$ and $\{\bar{1}33/3\bar{1}\bar{1}\}$ Cu $K\beta$. The experimentally determined δ_3's using the Gaussian distribution, (26), for $I_D(\Delta\varphi)$ agree with the theoretical δ_3 within 25°.

Table 1. *Experimentally determined phases* δ_3 [δ_3(*th.*): *theoretical value*]

(*a*) $\{11\bar{1}/113\}$ Cu $K\alpha_1$ [δ_3(th.) = 184°]

α(°)	δ_3 (max.)	δ_3 (min.)
0	193	183
10	195	183
20	204	183

(*b*) $\{11\bar{1}/113\}$ Cu $K\beta$ [δ_3(th.) = 184°]

α (°)	δ_3 (max.)	δ_3 (min.)
0	194	183
10	197	183
20	195	184

(*c*) $\{331/\bar{1}\bar{1}1\}$ Cu $K\beta$ [δ_3(th.) = 4°]

α (°)	δ_3 (max.)	δ_3 (min.)
0	3	−10
10	5	−11
20	8	−11

(*d*) $\{33\bar{1}/\bar{1}\bar{1}3\}$ Cu $K\beta$ [δ_3(th.) = 184°]

α (°)	δ_3 (max.)	δ_3 (min.)
0	194	183
10	200	184
20	206	183

4. Discussion and concluding remarks

In this study, the effects of the crystal boundary on the X-ray diffraction rely mainly on the crystal-surface inclination. It is well known that the two-beam diffraction intensity is inversely proportional to $|b|^{1/2}$

for strong reflection, where $b = \gamma_o/\gamma_G$. The inclination of the crystal used is checked by plotting the intensity of 333 *versus* φ of Cu $K\beta$. It gave well defined sinusoidal curves as expected. The error in the crystal cutting for the inclined surfaces was about $\pm 1°$.

For the inclined three-beam diffractions, the intensity variation due to the surface inclination is very large as can be seen in Figs. 2 and 3. The behavior of this variation was analyzed with the calculation procedure described in § 3. On the basis of geometric arguments, mirror symmetry is expected around 0 and 180°. In fact, by inspecting these figures, we readily detect some correlation between the reflections appearing in the interval 0–180° and those in 180–360°. For example, the I'_G peak intensity of the three-beam $L'/G'-L'$ diffraction at $\varphi+180°$ is the same as that of the three-beam $L/G-L$ diffraction at φ, where the secondary reflection L' of the former is the coupling $G-L$ reflection of the latter, and *vice versa*, *i.e.*

$$L/G-L \rightarrow G-L(-L')/L(=G'-L').$$

Referring to the theorem of reciprocity (see Pinsker, 1978; Chang, 1984), these two three-beam cases are equivalent. Consequently, the I'_G is the same for both three-beam cases. This explains why the two diffractions, being 180° apart in φ, have the same I'_G values.

As to the phase determination, it is evident that the sign of $\cos\delta_3$ associated with each three-beam diffraction investigated is clearly related to the asymmetry of the intensity profile obtained. This is consistent with the sign relation (Chang, 1981, 1982)

$$S(\cos\delta_3) = S_{LF}S_L \qquad (29)$$

where S_L is the sign of the profile asymmetry. S_L is positive if the left wing of the profile is higher than the right wing. S_L is negative for the reversed profile asymmetry. For the quantitative phase analysis, both Gaussian and Lorentzian distributions were adopted for $I_K(\Delta\varphi)$. Only the results from the Gaussian are listed in Table 1. It turned out that the Gaussian of (26) gave a better agreement between the experimentally determined δ_3 and the theoretical values. However, the difference in δ_3 between the Gaussian and the Lorentzian is less than 5°.

In conclusion, we have investigated the effect of the crystal-surface inclination on three-beam diffraction. The intensity variation caused by this inclination is understood to be governed by the resonance failures 2ξ's, namely, the excitation of the dispersion surface. The integrated intensity depends not only on the asymmetry parameter $b = \gamma_0/\gamma_G$ but also on γ_L. There seems no simple expression to describe the relation between the intensity and surface inclination. The overall effects of crystal inclination on diffraction intensity in the multibeam regime may have to be explained *via* dynamical calculation. On the other hand, the accuracy of the quantitative phase determination is not affected by the crystal-surface inclination, provided that the peak intensity $I'_G(\Delta\varphi=0)$ at $\Delta\varphi=0$ is treated as the maximum intensity for the kinematical intensity distribution $I_K(\Delta\varphi)$. For irregularly shaped crystals, the boundary conditions as well as the dynamical excitations of the dispersion surface are far more complicated than the surface-inclined crystals. To determine $I_K(\Delta\varphi)$ is the key to a reliable quantitative phase determination.

The authors are indebted to the National Science Council for financial support through grant no. NSC78-0208-M007-29. One of us (KCL) is also grateful to the same organization for providing a graduate fellowship during the course of this study.

References

BALTER, S., FELDMAN, R. & POST, B. (1971). *Phys. Rev. Lett.* **27**, 307–309.

BORRMANN, G. & HARTWIG, W. (1965). *Z. Kristallogr.* **121**, 401–409.

CAMPOS, C. & CHANG, S. L. (1986). *Acta Cryst.* A**42**, 348–352.

CHANG, S. L. (1981). *Appl. Phys.* A**26**, 221–226.

CHANG, S. L. (1982). *Phys. Rev. Lett.* **48**, 163–166.

CHANG, S. L. (1984). *Multiple Diffraction of X-rays in Crystals*, p. 134. Berlin: Springer-Verlag.

CHANG, S. L. & TANG, M. T. (1988). *Acta Cryst.* A**44**, 1065–1072.

CHANG, S. L. & VALLADARES, J. A. P. (1985). *Appl. Phys.* **37**, 57–64.

CHAPMAN, L. D., YODER, D. R. & COLELLA, R. (1981). *Phys. Rev. Lett.* **46**, 1578–1581.

COLE, H., CHAMBERS, R. W. & DUNN, H. M. (1962). *Acta Cryst.* **15**, 138–144.

COLELLA, R. (1974). *Acta Cryst.* A**30**, 413–423.

EWALD, P. P. & HENO, Y. (1968). *Acta Cryst.* A**24**, 5–15.

HART, M. & LANG, A. R. (1961). *Phys. Rev. Lett.* **7**, 120–121.

HILDEBRANDT, G. (1967). *Phys. Status Solidi*, **24**, 245–261.

HØIER, R. & AANESTAD, A. (1981). *Acta Cryst.* A**37**, 787–794.

HÜMMER, K. & BILLY, H. W. (1982). *Acta Cryst.* A**38**, 841–848.

HÜMMER, K. & BILLY, H. W. (1986). *Acta Cryst.* A**42**, 127–133.

HÜMMER, K., WECKERT, E. & BONDZA, H. (1989). *Acta Cryst.* A**45**, 182–187.

JAGODZINSKI, H. (1980). *Acta Cryst.* A**36**, 104–116.

JOKO, T. & FUKUHARA, A. (1967). *J. Phys. Soc. Jpn*, **22**, 597–604.

JURETSCHKE, H. J. (1982*a*). *Phys. Rev. Lett.* **48**, 1487–1489.

JURETSCHKE, H. J. (1982*b*). *Phys. Lett. A*, **92**, 183–185.

KOV'EV, E. K. & DEIGEN, M. I. (1987). *Sov. Phys. Crystallogr.* **32**(2), 176–177.

MO, F., HAUBACH, B. C. & THORKILDSEN, G. (1988). *Acta Chem. Scand. Ser. A*, **42**, 130–138.

PINSKER, Z. G. (1978). *Dynamical Scattering of X-rays in Crystals*, p. 481. Berlin: Springer-Verlag.

POST, B. (1977). *Phys. Rev. Lett.* **39**, 760–763.

POST, B. (1983). *Acta Cryst.* A**39**, 711–718.

POST, B., CHANG, S. L. & HUANG, T. C. (1977). *Acta Cryst.* A**33**, 90–98.

POST, B., NICOLOSI, J. & LADELL, J. (1984). *Acta Cryst.* A**40**, 684–688.

RENNINGER, M. (1937). *Z. Phys.* **106**, 141–176.

SACCOCIO, E. J. & ZAJAC, A. (1965). *Acta Cryst.* **18**, 478–480.

SHEN, Q. (1986). *Acta Cryst.* A**42**, 525–533.

SHEN, Q. & COLELLA, R. (1988). *Acta Cryst.* A**44**, 17–21.

TANG, M. T. & CHANG, S. L. (1988). *Acta Cryst.* A**44**, 1073–1078.

THORKILDSEN, G. (1987). *Acta Cryst.* A**43**, 361–369.

UEBACH, E. & HILDEBRANDT, G. (1969). *Z. Kristallogr.* **129**, 1–8.

UMENO, M. & HILDEBRANDT, G. (1975). *Phys. Status Solidi A*, **31**, 583–594.